Binary-collision-cascade simulation of hyperchanneling of high-energy helium ions in silicon

C. S. Murthy and G. R. Srinivasan
Theoretical Modeling Department, IBM Semiconductor Research and Development Center, East Fishkill, Z/47C, Hopewell Junction, New York 12533
(Received 2 March 1992; revised manuscript received 29 June 1992)

The binary-collision-cascade code, MARLOWE, was modified to include an accurate electron-density distribution of silicon and an electronic-energy-loss (EEL) model that is suitable for high-energy studies. The EEL model is based on a theory that relates the energy loss and local valence-electron density via a phenomenological band-structure model. The enhanced MARLOWE is applied to simulate transmission spectra due to the hyperchanneling of high-energy α particles in silicon along the [110] and [111] directions. The transmission spectra due to a "random" incident direction was also studied. The channeling peak positions in the energy-transmission spectra agree fairly well with the measurements. The effects of transverse-energy distribution of the incident beam, the effects of electron-multiple scattering and energy-loss straggling, and the effects of nonuniformity of the electron density on the transmission spectra are discussed. The electron-density effects reproduce the stopping-power measurements based on the peak and leading edge of the energy spectrum. The importance of energy-loss straggling, of core-electron contribution to the energy loss at high energies, and of charge-state effects at intermediate energies is also discussed.

I. INTRODUCTION

Study of the energy loss of channeled particles was given much attention in the late 1960s (Refs. 1 and 2) in order to elucidate the channeling features and the energy-loss mechanisms, and to interpret backscattering experiments and the electron-density variation in crystals. These investigations have resulted in the measurement of the energy distribution of the transmitted particles and of the accurate stopping-power data for energetic light ions in silicon.[3–7] Additionally, this had stimulated much theoretical activity[2,8–15] in these areas, especially around the higher-energy region ($E > 1$ MeV), and the ion-motion calculations mostly involved either a continuous effective potential due to the atomic rows and planes in the lattice or only the central region of the channel.

Ion-transmission spectra provided a convenient means for the examination of the electronic-energy-loss (EEL) models which can then be adapted to simulate technologically important ion implantation phenomena which is useful for very large scale integrated (VLSI) technology, not only for modern shallow device structures at lower energies but also for deep implants, especially with regard to the channeling tail and implant damage. One of the techniques that models both these effects is the simulation of ion-collision cascades in the crystalline solid using an appropriate treatment for the collision dynamics. There are several simulators, MARLOWE,[16–18] and other recent programs[19–22] which do this to varying levels of sophistication.

MARLOWE was developed by Robinson and co-workers at the Oak Ridge National Laboratory to simulate collision processes in crystalline solids. The many-body dynamics that is inherent for simulating the slowing down of energetic atoms in solids[23–25] is reduced to a binary collision dynamics, which is expected to be valid from 0.1 keV to several MeV incident energy range, the lower and upper limits being governed by the binary collision restriction and the neglect of relativistic effects, respectively. MARLOWE uses the binary collision approximation (BCA) to compute the trajectory of a moving particle as it makes its way through the crystal. Simultaneous collisions are accounted for in an approximate manner.[16–18] Each collision event is assumed to be composed of a quasielastic (nuclear) component and inelastic (electron excitation) component. MARLOWE provides many options which include different target structures, multilayer targets, choice of interatomic potentials, and EEL models to model more closely a variety of situations. The Monte Carlo sampling is used to generate successive particles with regard to their initial position. We have added to MARLOWE a variety of different postprocessors[26] for the analysis of the data. While we will not describe all these options (the reader is referred to Refs. 17–19), we will discuss in some detail the available options for the electronic energy losses with which we are concerned in the present investigation.

Previous phenomenological EEL models[27–29] that were available in MARLOWE do not include an explicit dependence of electronic stopping on the target electron density. More recent EEL models[30,31] consider isotropic charge distribution, expressed in terms of the one-electron shell radius based on Brandt's effective stopping-power charge for metals,[32,33] around the target atoms. While these models may be appropriate for metallic targets, they are unlikely to model accurately[26,30,31] the energy losses in crystals with highly anisotropic charge distributions as in silicon. The EEL model of Burenkov, Komarov, and Kumakhov (BKK),[12] which is appropriate for nonuniform electron density, is used in the present work.

We used the hyperchanneling[34] studies, where the

beam is highly aligned to the prominent channeling direction in silicon to within $\pm 0.01°$, as a stringent criterion for testing the BKK model for MeV-energetic light ions such as protons, α particles, and He ions, as these projectiles slow down mostly by the electronic stopping in this energy range. Also, the availability of good transmission data for these cases allows us to make a quantitative examination of the simulation technique. We thus undertook a detailed application of the BCA technique to a study of the hyperchanneling transmission spectra of high-energy α particles in silicon.

We have incorporated into MARLOWE BKK's analytical expression which is appropriate for high-velocity projectiles. Details of this model and the necessary input for the silicon electron-density distribution as obtained by the x-ray structure factor data are discussed in the next section. The remainder of the paper is organized as follows: Discussion of the results of simulated energy-transmission spectra is included in Sec. III, and Sec. IV summarizes the findings.

II. ELECTRONIC STOPPING POWER

Electronic stopping power comprises the energy loss due to the valence electrons (plasmon and single-particle excitations) and core electrons. The former dominates in the energy range 0.1–4 MeV, while above this energy range the latter becomes important. BKK (Ref. 12) have extended the EEL model of De Salvo and co-workers[8–10] for fast-channeled ions in crystalline materials, which includes the spatial nonuniformity of valence-electron density. While this theory takes into account the nonuniform valence-electron-density distribution in calculating the stopping power, question may arise as to the exactness of the local-density formalism used here. Nevertheless, due to the demonstrated agreement[12,35] with the stopping-power measurements, we proceed with this approach. Here we give a brief description of this EEL model.

A. Theory

Based on the dielectric response formalism, together with the use of an effective potential to account for the local-field effects, De Salvo and co-workers[8–10] have derived a relation between the channeling ion energy loss and the local valence-electron density. Their expression for the energy loss of a particle with charge Z_i and velocity V in a crystalline medium of nonuniform electron density takes the form

$$S_e(\mathbf{r})=\frac{Z_i^2e^2}{\pi^2V}\int\frac{d^3q}{q^2}\int d\omega\,\omega\sum_{\mathbf{G}}\mathrm{Im}[K_{\mathbf{G},0}(\mathbf{q},\omega)]\times e^{i\mathbf{G}\cdot\mathbf{r}}\delta(\omega-\mathbf{q}v)\ , \quad (1)$$

where $K_{\mathbf{G},0}(\mathbf{q},\omega)$ is the inverse dielectric matrix which depends on frequency ω and wave vector $\mathbf{q}$, and $\mathbf{G}$ is the reciprocal-lattice vector. The inverse dielectric matrix elements satisfy the relation

$$\sum_{\mathbf{G}''}\varepsilon_{\mathbf{G},\mathbf{G}''}(\mathbf{q},\omega)K_{\mathbf{G}'',\mathbf{G}'}(\mathbf{q},\omega)=\delta_{\mathbf{G},\mathbf{G}'}\ . \quad (2)$$

The component $\varepsilon_{0,0}$ corresponds to the conventional (i.e., uniform electron-gas) dielectric function $\varepsilon(\mathbf{q},\omega)$. The off-diagonal terms $\varepsilon_{\mathbf{G},\mathbf{G}'}$ represent the components along various crystallographic directions.

The calculation of $S_e(\mathbf{r})$ thus requires an evaluation of dielectric function $\varepsilon_{\mathbf{G}}(\mathbf{q},\omega)$ within a wide range of $\mathbf{q}$ and ω for several $\mathbf{G}$ vectors. In order to make it computationally tractable, BKK used a simple model for the crystal band structure, and after several manipulations they expressed the energy loss of charged particles in a crystal as a Fourier series of the stopping power for reciprocal-lattice vectors, $\mathbf{G}$, as

$$S_e(\mathbf{r})=\sum_{\mathbf{G}}S(\mathbf{G})e^{i\mathbf{G}\cdot\mathbf{r}}\ , \quad (3a)$$

where

$$S(\mathbf{G})=\frac{Z_i^2e^2}{\pi^2V^2}\int_0^{\infty}\frac{dq}{q}\int_0^{qV}d\omega\,\omega\frac{-\varepsilon_2}{\varepsilon_1^2+\varepsilon_2^2}f(\mathbf{G})\times\int_0^{2\pi}\hat{e}(\mathbf{q})\hat{e}(\mathbf{q}+\mathbf{G})d\phi\ , \quad (3b)$$

and where ε_1 and ε_2 are the real and imaginary parts of the dielectric response function, $f(\mathbf{G})$ is the Fourier component of the valence-electron density in a crystal which is normalized so that $f(0)=1$, $\hat{\mathbf{e}}(q)$ is the unit vector in the direction $\mathbf{q}$, and ϕ is the azimuthal angle from the direction of the vector $\mathbf{G}$ in the spherical coordinate system for the wave vector $\mathbf{q}$. Using the analytical expressions for the dielectric functions ε_1 and ε_2 given in their paper, the energy loss can be obtained from Eqs. (3) down to the low-energy regime. Details of the evaluation of $S(\mathbf{G})$ and the behavior of the integrand in Eqs. (3) are discussed elsewhere.[35]

For velocities much higher than the Fermi velocity, $V\gg V_F$, various approximations were made by BKK to reduce the integrals in Eqs. (3) to a simple analytic expression which relates the energy loss and the valence-electron density in the crystal, as given by

$$S_e(\mathbf{r})=\frac{Z_i^2e^2\omega_p^2}{V^2}\left[\{\tfrac{1}{2}+\tfrac{1}{2}\rho(\mathbf{r})\}\ln\frac{2mV^2}{\hbar\omega_p}+\tfrac{1}{2}\sum_{\mathbf{G}\neq0}f(\mathbf{G})e^{i\mathbf{G}\cdot\mathbf{r}}\ln\frac{2m\omega_p}{\hbar G^2}\right]\ , \quad (4)$$

where

$$\rho(\mathbf{r})=1+\sum_{\mathbf{G}\neq0}f(\mathbf{G})e^{i\mathbf{G}\cdot\mathbf{r}} \quad (5)$$

is the normalized density of valence electrons at a given point $\mathbf{r}$, $\omega_p=\sqrt{4\pi\rho e^2/m_e}$ is the plasma frequency, and m_e is the electron rest mass. Equation (4) can be used to determine the stopping power of an ion, knowing $f(\mathbf{G})$, provided $V\gg V_F$.

The zeroth Fourier component of Eqs. (3) or (4) gives the energy loss in a medium of uniform electron gas which may correspond to the maximum in the energy spectrum, representing the most probable energy loss.[12] The best-channeled particles, on the other hand, contribute to the leading edge of the spectrum where $\rho(r)$ variation from Eq. (5) applies.

B. Computational details

The energy losses of helium ions channeled through silicon have been studied[5,6] by measuring the energy-transmission spectra. Eisen *et al.*[5] have carried out detailed investigation in order to determine both channeled and random stopping of helium in silicon over a wide energy range from about 0.1 to 18 MeV. In addition, they provide the transmitted energy spectra for the 7-MeV helium beam. For 7 MeV, which is $\simeq 75$ times the *energy* (93 keV) of α particles corresponding to the Fermi velocity V_F (equivalently, in terms of *velocity,* 7-MeV energy of α particles corresponds to $\simeq 8.7V_F$), BKK's analytical expression [Eq. (4)] is appropriate and was implemented in MARLOWE. The silicon valence-electron density as evaluated from the x-ray structure-factor data (values in the last column of Table IV of Ref. 36) was inserted into the namelists of MARLOWE for the six reciprocal-lattice vectors **G**, namely (111), (220), (222), (311), (400), and (422). In each case the appropriate signs for the set of equivalent directions corresponding to each major lattice direction were determined by symmetry considerations.[37] For higher **G** values, the valence-electron structure factor becomes very small and was not included. The valence structure factors used are those obtained by subtracting the structure factor for core electrons (values in the second column of Table IV in Ref. 38) from the experimental values compiled by Raccah *et al.*[39] as the most reliable set. Although other structure-factor sets are also used for investigating the effects of different structure-factor input which will be discussed later, we report mostly the results obtained with this set.

Thermal vibrations corresponding to 300 K, based on the Debye model, are included using a value of 643 K for the silicon Debye temperature. For the nuclear stopping treatment in the enhanced MARLOWE, we have used the Molière approximation to the Thomas-Fermi (TF) potential. The scattering of the projectiles was evaluated for all events with impact parameters less than a cutoff value (b_c). The choice of b_c is discussed later.

An option to take into account the spread in the energy of the incident beam was also added. A triangular-shaped energy spread is used, where the vertex of the triangle is at the required incident-beam energy (7 MeV) and the spread in the energy is the base of the triangle. An energy spread of 77 keV, based on the measured half-width of the incident beam, is used in our calculations.

The ion trajectory was divided into small segments and the electron densities and the energy loss along the segment were calculated. We calculated the total electronic stopping by integrating the energy loss for various segments in the collision trajectory. The choice of the step size for dividing the ion path into segments was examined in terms of convergence of the peak position. The shape of the energy distribution did not vary significantly with the step size. However, when only one segment was used for the entire collision path, the results were unphysical, especially for the ⟨111⟩ channeling spectra.

III. RESULTS AND DISCUSSION

With the use of experimentally determined silicon electron-density distribution, the simulation was run for ⟨110⟩ and ⟨111⟩ channels to obtain the energy-transmission spectra of 7-MeV α particles in 11.2-μm-thick silicon crystal, used in Eisen's experiment.[5] In order to match the experimental conditions, we used an angular divergence of $\pm 0.03°$ for the α-particle beam. A comparison of these simulation results with the experimental data is shown in Fig. 1 for the ⟨110⟩ and ⟨111⟩ hyperchannels. Also shown is the effect of the beam tilt away from the channel to a "random" orientation on the transmission spectra. Typically, these simulations were made for 1200 particles. While the simulations that include inhomogeneity of the electron density typically took about 100 h of CPU time on the IBM 3090/600E and similar time on the IBM RISC 6000–Model 520, the runs with the contribution exclusively from uniform-electron density required 20 h CPU time.

We believe that this is the first time a detailed collision cascade approach has been applied for simulating transmission spectra due to hyperchanneling. From Fig. 1 we see that the simulated peak positions of the spectra for ⟨110⟩ and ⟨111⟩ channels match those from the measurements. We also note that the ⟨111⟩ simulated spectrum is narrower compared to the simulated ⟨110⟩ hyperchannel spectrum. This relative difference in the spectral shape for the two hyperchannels is similar to that found in the measured spectra. However, the observed spectral features of the hyperchannels such as shape and half-width are not reproduced in the simulations. We discuss below these discrepancies in terms of MARLOWE input variations, energy-loss straggling, and core-electron contribution to the energy loss.

In order to simulate the so-called random spectrum, we tilted the [110] and [111] beams and obtained the transmission spectra as a function of angular tilt. In Fig. 1 we show the spectrum for a tilt of 17°, which is sufficiently away from any major crystallographic channeling direction to represent a typical "random" implant. It was found that as the angular tilt from both [110] and [111] is increased, the simulated peaks move toward the random peak. At 17° tilt, the simulated peak position is the same for tilts both from [110] and [111]. Based on these simulations, we note that the enhanced MARLOWE can reproduce the experimentally observed shift in the

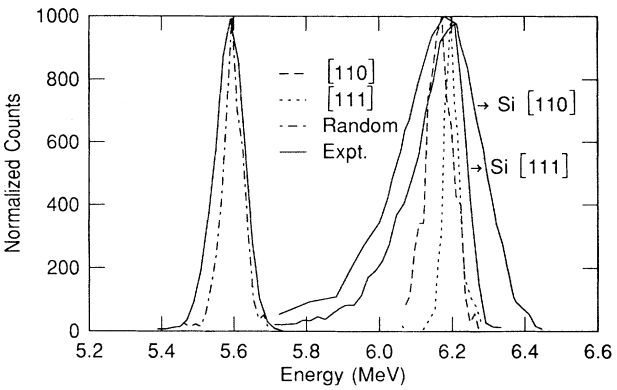

FIG. 1. Simulated and experimental transmitted energy distributions for polychromatic 7-MeV α-particle beam through a 11.2-μm-thick Si crystal for [110], [111], and random directions.

peak from the hyperchannel position to the random position in the transmission spectrum for the α particles implanted into the thin silicon crystal. The shape and half-width of the simulated spectra are in better agreement with measurements for the random peak than for the channeled peaks.

In order to examine the discrepancy in the shape and half-widths for the hyperchannel spectra, we considered the following: (a) effects of energy spread in the incident beam, (b) dependence on the variation in scattering parameters, (c) variations in the structure factor input which in turn affects the electron density and the energy loss, (d) electron-multiple scattering, and (e) energy-loss straggling effects. These are described below.

A. Incident energy-spread effects

Eisen *et al.*[5] have discussed the effect of incident energy spread based on their measurements and some unpublished experimental data on MeV-energy protons in Ge to explain the differences in the spectral widths for the different channels. They conclude that the spectral features are governed partly by the transverse energy distribution of the incident particles and partly by the influence of the stopping power on the transverse energy of the channeled ions.

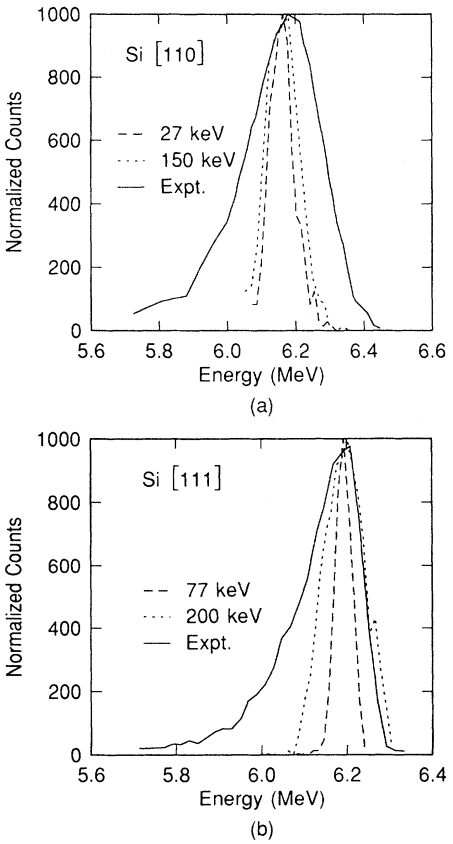

FIG. 2. Effects of energy spread in the 7-MeV incident beam on the energy-transmission spectra for 11.2-μm-thick Si crystal in (a) [110] and (b) [111] directions. Experimental spectrum (half-width on the incident beam is $\sim$77 keV) is also shown for comparison.

Figures 2(a) and 2(b) show the transmitted energy spectra simulated for [110] and [111] directions as the energy spread in the incident beam was varied from 27 to 200 keV. The half-width of the experimental incident beam is $\sim$77 keV. We used a triangular energy-spread distribution for the incident beam which may differ from the experimental incident-beam distribution. While the half-width of the simulated spectrum is shown to depend on the energy spread of the incident beam for both the $\langle 110 \rangle$ and $\langle 111 \rangle$ axial channels, the energy-spread effect on the spectral broadening is significantly more for the $\langle 111 \rangle$ hyperchannel than for the $\langle 110 \rangle$ channel, while both are considerably smaller than the experimental value.

B. Scattering parameter effects

We now turn our attention to the effect of impact parameter cutoff (b_c) on the stopping power. In MARLOWE, ion encounters with impact parameters larger than b_c are ignored. We have found in our previous simulations,[26] when the valence-electron density was calculated once along each ion trajectory for each collision, the $\langle 110 \rangle$ transmission spectra showed subsidiary peaks. We also had difficulty in obtaining a reasonable spectrum for the $\langle 111 \rangle$ orientation. This led to an examination of the sensitivity of the $\langle 110 \rangle$ transmission spectra to the choice of b_c and the simultaneous collision parameters. As b_c decreases, which makes the corrections for simultaneous collisions less important, the peak of the spectrum shifted significantly to lower energies.

In the present implementation of BKK's EEL model we used low b_c values, 0.0543 ($=0.1a$, where a is the lattice parameter of silicon) and 0.1086 nm, both of which are larger than the value (0.003 nm) that is indicated by nuclear scattering integral tables or the Rutherford cross section for 7-MeV α particles.[40] We recognize, however, that these cutoffs are much smaller than the Bohr's adiabatic radius (0.45 nm for a 7-MeV beam) which is the effective cutoff radius for the inelastic processes. When a large value of b_c (0.233 nm) was used, the subsidiary peaks appeared and the spectral features became sensitive to the choice of the simultaneous collision parameters. With the lower b_c values, we do not see any secondary peaks. While the peak position shifts to a lower energy by about 2.2%, as b_c is decreased from 0.233 to 0.0543 nm, the spectral half-width reduces by about 25%. Here we note that the half-width estimates are approximate because even the use of larger b_c underestimates the half-width by nearly 50% compared to the measurement. This decrease of energy loss as the impact parameter increases is in accordance with earlier theoretical investigations.[7,13] In the absence of any further theoretical justification, we have opted to use a low value of b_c. Also, we note that for larger b_c's (approaching Bohr's adiabatic radius), when the ion path is near midchannel for the $\langle 110 \rangle$ orientation, we need a more exact treatment of the simultaneous collisions than is provided for in MARLOWE. We consider other effects due to electron-density variations, energy-loss straggling, and core contributions for the broadening of the peak.

C. Uniform vs nonuniform electron-density effects

As mentioned earlier, at high energies the uniform-electron-density approach is a reasonable approximation for characterizing the maximum in the spectrum which corresponds to the most probable energy loss. On the other hand, for the best-channeled particles the electron density must be calculated from Eq. (5) and the leading edge of the spectrum should be used.

We performed the simulation both with the zeroth Fourier component (uniform electron gas) in the energy-loss expression [Eq. (4)], which can be expected to correspond to the peak maximum, and with the inclusion of inhomogeneity of the electron density (i.e., $\mathbf{G}\neq 0$) which is for the leading-edge spectrum. These results are shown in Figs. 3(a) and 3(b) for both [110] and [111] directions. Clearly in the case of the ⟨110⟩ channel, the maximum in the energy spectrum shifted to lower energies for the uniform electron-gas calculation compared to the best-channeled situation, while there is a negligible shift for the case of the ⟨111⟩ channel spectra. These effects are consistent with the experimental observation of Eisen *et al.*[5] Although Eisen *et al.* did not show the transmission spectra distinguishing the maximum and leading edge of the energy distribution, they had reported the stopping-power data for both the peak maximum and leading edge separately for various channels. Thus we observe a significant difference between the [110] and [111] cases for both the leading edge and peak maximum.

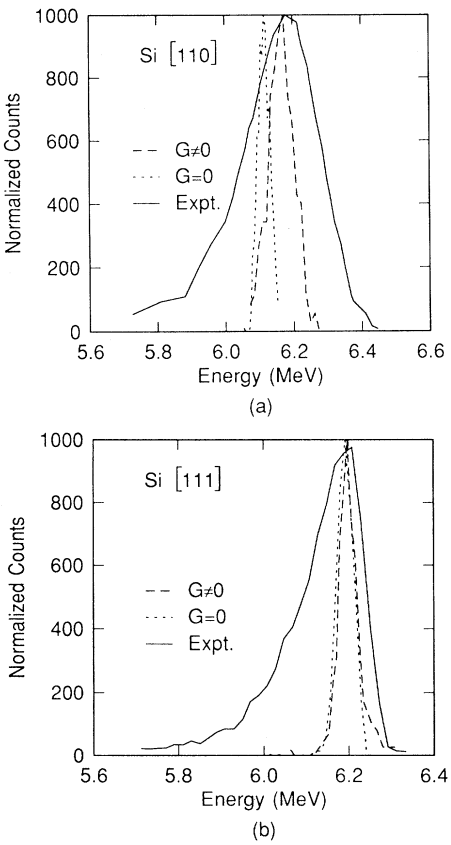

FIG. 3. Comparison of the experimental energy distribution and simulated energy-transmission spectra with uniform gas of valence electrons ($\mathbf{G}=0$) and the inclusion of nonuniform electron density variation in the ion path ($\mathbf{G}\neq 0$). (a) 7 MeV α particles→11.2-μm-thick Si(110). (b) Same as in (a) with Si(111).

By comparing the spectra of the ⟨110⟩ and ⟨111⟩ channels for $\mathbf{G}=0$ (uniform electron gas) and for $\mathbf{G}\neq 0$ (nonuniform electron distribution in the channel) we make the following observation from Figs. 3(a) and 3(b). The $\mathbf{G}=0$ and $\mathbf{G}\neq 0$ spectra are nearly identical for the ⟨111⟩ channel. We interpret this as due to the fact that the only structure-factor contribution to electron-density nonuniformity in the ⟨111⟩ peak comes from {220}, which are much smaller than that for $f(\mathbf{G}=0)$. However, for the ⟨110⟩ channel, the $\mathbf{G}\neq 0$ contribution is larger than that for $\mathbf{G}=0$. This is because many stopping-power Fourier components contribute significantly to the total stopping power for the ⟨110⟩ channel, unlike for the ⟨111⟩ channel. These results also show that electron-density inhomogeneities influence the half-width more than the peak position. This may be due to the fact that the variation of the electron-density gradient near the more open ⟨110⟩ channel is larger than that for the ⟨111⟩ channel.

D. Structure-factor effects

There is a large spread in the structure-factor data for silicon. There are several structure-factor sets[36,38,39,41] based on pseudopotentials. Scheringer[42] had recently analyzed the various experimental structure-factor data sets and had compiled a corrected set by accounting for the anomalous dispersion for *pendellösung* data. We used the set by Bertoni *et al.*[36] because their calculations yield directly the structure factors for valence electrons which eliminates some uncertainties in subtracting the core-electron contribution. As an alternate source to that compiled previously by Raccah *et al.*[39] for the observed structure factors, we used the latest compilation by Scheringer,[42] from which the core-electron contribution (values in the second column of Table IV of Ref. 38) was subtracted to obtain the valence-electron structure factors.

For comparison, we calculated the energy-transmission spectra with three different valence-electron structure-factor inputs: (a) Raccah *et al.*,[39] (b) Bertoni *et al.*,[36] and (c) Scherringer.[42] Due to the intense CPU time requirements, simulations with sets (b) and (c) consisted typically of 350 particles. We found that while the half-width of the transmission-energy spectrum changes by about 12% for set (c) and 5% for set (b), the peak shifts to lower energies by about 0.5–1% with reference to set (a). As noted before, the half-width estimates are approximate. It was found that peak positions are more sensitive to the variation in the structure-factor input for the ⟨110⟩ channel than for the ⟨111⟩ axial channel. Valence structure factors corresponding to set (c) led to the lowest ($\simeq 1\%$) energy peak shift for ⟨110⟩. This reduction relates to the structure-factor values for the (111) $\mathbf{G}$ vector, the dominant contributor after the (000) vector to the energy loss. The normalized $[f(0)=1]$ values are -0.29, -0.218, and -0.1965 for the sets (a), (b), and (c), respectively. Although for higher $\mathbf{G}$ values, such as (400) and (422), the valence structure factors corresponding to set

(c) are significantly large relative to sets (a) and (b), we found that the energy spectrum is not sensitive to these changes in the structure factors, thus indicating that the contribution from higher **G** values to the total energy loss is not significant.

E. Electron-multiple scattering

While MARLOWE accounts for the multiple scattering of the ions by the nuclear interactions, there is no option either in MARLOWE or in the implemented energy-loss model to deal with the electronic multiple-scattering effects. However, a rough estimate of the mean-square scattering angle from the electrons can be estimated by the expression[43] which is valid in the high-velocity limit as

$$\langle \theta^2 \rangle = \frac{m_e}{2m_i} \frac{\Delta E}{E} , \tag{6}$$

where m_i is the projectile mass, E is the incident energy, and ΔE is the energy loss. Using the mean energy loss from the energy distributions of the hyperchannel spectra, the root-mean-square scattering angle is $\sim 0.008°$. The angular aspect of multiple scattering is thus likely to be unimportant, since the scattering by electrons must lead to much smaller deflections than the scattering by the target nuclei. But the fluctuations in the electronic energy loss (straggling) may not be negligible, especially since the electronic energy loss is the major mechanism of slowing down of highly energetic α particles. This will be considered next.

F. Energy-loss straggling

In a strictly local picture of the EEL, one might argue that energy-loss-fluctuation results from fluctuations of the electron density along the track of any one projectile, and the resultant effect of many-projectile trajectories, is implicitly included. As the implemented EEL model is not a strictly local model, effects due to the energy-loss straggling must be included. Although energy-loss straggling is a second-order effect, numerous theoretical investigations are continually pursued[44–51] to include correlation effects within the electron bunch in the target species and the charge-state fluctuations.[49–51] Theories consistently underestimate the experimental data on energy-loss straggling. Except for the charge-state fluctuations, which are not important at high energies, electron correlation effects can be accounted for in any computer simulation provided that the straggling is included in simulating ion trajectories. Such an "*in situ*" calculation is not attempted here. Instead a rough estimate of straggling, Ω^2, was made based on an available expression[43] for the relative straggling.

Based on the TF model for target atoms with high atomic number ($Z_t > 10$), Lindhard and Scharff[44] have obtained the following expression for the relative straggling:

$$\frac{\Omega^2}{\Delta E} \simeq \begin{cases} E\dfrac{m_e}{m_i}, & x \le 3 \\ E\dfrac{2}{L(x)}\dfrac{m_e}{m_i}, & x > 3 \end{cases} , \tag{7}$$

where x is the dimensionless energy parameter given by

$$x = V^2/V_B^2 Z_t , \tag{8}$$

V_B is the Bohr velocity, and $L(x)$ is the Lindhard-Scharff universal function

$$L(x) = 1.36x^{1/2} - 0.016x^{3/2} . \tag{9}$$

Using the mean energy loss obtained from the random, (110), and (111) energy distributions, Ω^2 is estimated to be, respectively, 0.938, 0.558, and 0.538×10^{-3} MeV^2, which leads to 61%, 19%, and 41% increases in half-width, respectively, assuming a Gaussian distribution for the energy-loss probability. In the case of random spectra the increased half-width due to the inclusion of either the above estimate or the Bohr's estimate of 0.816×10^{-3} MeV^2 resulted in a close agreement with the experiment. This is not surprising because the above formulation is based on a uniform electron-gas model target and is thus readily applicable for random spectra. For hyperchannel spectra, these estimates can be considered at best to be the lower bound for straggling, as the use of accurate electron densities pertaining to the atom in the crystal led to higher straggling ($> 10\%$).[47–49] Although it is difficult to estimate quantitatively the straggling and its effect on the transmission spectra without actually including the straggling effects in simulating the ion trajectories, these rough estimates do indicate that at least 23–50% of discrepancies in the half-widths can be accounted for in terms of the straggling effects depending on the hyperchannel. We are proceeding to include these effects and plan to communicate the results in the near future.

G. Valence- and core-electron effects

The spectral shape of the hyperchannels are not well reproduced for the on-axis transmission spectra compared to that for the random spectrum, as discussed earlier. However, our simulations are successful in predicting that the ⟨111⟩ spectrum is narrower than the ⟨110⟩ spectrum, as observed experimentally. Furthermore, the half-width corresponding to the ⟨110⟩ spectrum calculated with uniform electron density is quite a bit narrower than that obtained by the inclusion of the inhomogeneity of the electron density. Thus the spread in the transmission spectra is shown to depend on the nonuniformity of electron density within the channel, and a representation involving only the valence electrons in the channeling situation may lead to a less realistic electron-density variation in the channel, especially at low impact parameters. The BKK theory includes only the contribution of valence electrons, whereas for the 7-MeV α-particle beam the core electrons may contribute to the energy loss. We now consider the possible effect of core electrons on the energy distribution.

On the basis of the channel radius and the estimates of critical impact parameters for 4-MeV protons obtained from the binding energy of the inner shell (L) electrons, Dettmann and Robinson[13] have shown that at high energies core electrons would contribute more to the stopping power for the ⟨111⟩ channel than to the ⟨110⟩ channel.

This implies that the core contribution may affect the position of the peak of the ⟨111⟩ channel energy-transmission spectrum more than that of the ⟨110⟩ channel. However, as the variation of the electron-density gradient near the ⟨110⟩ channel is larger than in the ⟨111⟩ channel, we expect that the core effects are more for the ⟨110⟩ channel half-width than for the ⟨111⟩ channel. This reasoning is consistent with the data shown in Figs. 3(a) and 3(b). Also, the core contribution for the random peak at this energy could be as large as 50%.[52] Although there have been several attempts[12–15,53] to include the core-electron contributions to the stopping power, we have not yet made a quantitative estimate of the core-electron effects. Instead, we select a simulation at a lower energy for which measurements are available and for which core contributions are expected to be small.

Bulgakov, Nikolaev, and Shugla[7] carried out measurements for 1.3-MeV He ions transmitted through 2.5-μm-thick silicon crystal for the ⟨110⟩ axial, {111}, and {110} planar channels. The measured energy spectrum for the ⟨110⟩ channel peaks at about 0.8 MeV with a half-width of about 0.16 MeV. Figure 4 shows the experimental spectrum as normalized to the peak value of the simulated spectrum. In order to match the experimental conditions, we used an angular divergence of $\pm 0.03°$ for the He beam and an energy spread of 55 keV. The impact parameter was cut off at 0.1086 nm. Our simulations with the analytical Eq. (4) for fully ionized particles [i.e., $Z_i=2$ for He in Eq. (4)] gave a peak value of 0.67 MeV for the transmission spectrum with the half-width of about 0.13 MeV, as shown in Fig. 4. The energy-loss straggling, based on Eq. (10), is 1.088×10^{-4} MeV^2. We found that both this value and Bohr's estimate of 1.822×10^{-4} MeV^2 do not contribute significantly to the spectral half-width. We find that the half-width is fairly

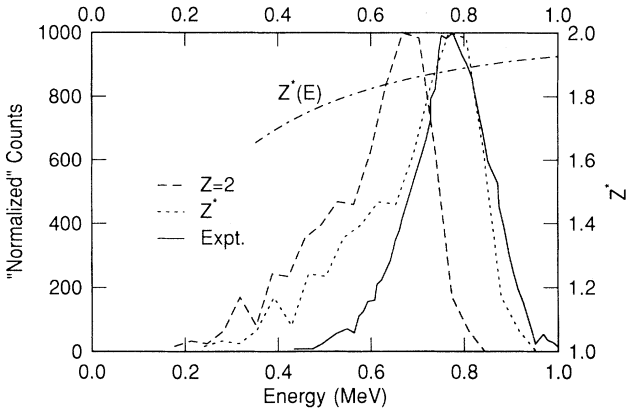

FIG. 4. Comparison of the experimental and simulated (both for the fully ionized beam and varying charge states) energy transmission spectra for polychromatic 1.3-MeV α-particle beam through a 2.5-μm-thick Si crystal along the ⟨110⟩ axial channel. The variation of effective charge (Z^*, ordinate scale on right side of figure) with energy is also shown. The label "normalized" refers to the adjustment of the experimental relative units to that of simulation.

reproduced, while the simulated peak position is lower than in the experiment. Part of the discrepancy could be due to the fact that the analytical Eq. (4) departs from detailed integration of Eq. (3) at intermediate and low energies, which produces an overestimation of the stopping power.[35] Also, it is expected that at or below 4 MeV the effect of the charge states of the projectile have to be taken into account. Thus Z_i could be <2 and a fixed value of $Z=2$ would also overestimate the stopping power, which would result in the shifting of the energy-transmission spectrum to lower energies compared to the measurements. This point will be considered next.

H. Charge-state effects

There have been studies[54–57] to account for the charge-state effects in terms of an effective charge parameter. One approach has been to use the TF description of electron charge around the moving ion and to relate the degree of ionization to the velocity of the ion. This treatment was seen to be adequate[56] for heavy ions ($Z>6$), as can be expected by using the TF model. Although improvements to this approach exist,[32,33] the applicability of the TF description to He ions remains in doubt. While more recent first-principles calculations[58] are best suited for this purpose, such an approach would be difficult because of the CPU complexity of treating thousands of ion trajectories with these calculations. An alternate recourse is to use either statistical estimates[35] based on Bohr's stripping criterion[59] and the projectile's electron density or the empirical models that were proposed[54–56] based on fitting a large set of experimental data. For instance, Williamson, Boujot, and Picard[55] defined the effective nuclear charge as $Z_i^*=\gamma Z_i$ where $\gamma=\tanh[137\sqrt{(\pi/2)}V_i/cZ_i]$, c being the speed of light in vacuum. For the energies of interest in the present application (0.45–1.0 MeV), Z^* varies from ~ 1.6 to 1.9 instead of 2, which is for the fully ionized He ion. The typical variation of Z^* with energy is also shown in Fig. 4, using this model.

Considering Z^* as a mere scaling factor at this stage, and using the above expression for Z^*, we updated the electronic stopping based on the energy distribution for $Z=2$. The new energy spectrum, which takes into account empirically the charge-state effects, is also shown in Fig. 4. It is quite encouraging to see that the simulated peak agrees closely with the measurement. The spectrum, however, is broader at the lower energy, spreading up to 0.2 MeV. As energy decreases, the BKK approximations made in Eq. (4) become questionable. Studies involving the full integral in Eq. (3) and more realistic charge-state effects are in progress for low-energy He and B ion-transmission spectra, and some preliminary results have been reported elsewhere.[60]

IV. SUMMARY

Detailed collision cascade simulations have been carried out for the MeV-energy range α-particles transmission through thick silicon crystal by using the full Si electron-density distribution and appropriate EEL (BKK) model. The effects of electron-density inhomogeneity are

in good agreement with stopping-power measurements for the peak maximum and leading edge of the spectrum. The enhanced version of MARLOWE can reproduce hyperchannel peak positions for 7-MeV α particles in both the $\langle 110 \rangle$ and $\langle 111 \rangle$ axial channels. Our detailed analyses in terms of varying the simulation parameters, such as impact parameter cutoff, energy spread in the incident beam, and structure factor input, have shown that, although these effects do influence the spectral features, none of them nor their combined effect can account for the narrowness of the simulated spectra for 7-MeV α particles in comparison with measured spectra for the axial channels. The discrepancy in the spectral features of the 7-MeV energy range may partially be due to the neglect of energy-loss straggling effects and of core-electron contribution to the energy loss. The inclusion of charge-state effects brought better agreement with experiment for 1.3-MeV He ions. Moreover, in the case of highly energetic light particles, the scattering angles become very small and quantum-mechanical effects[61] may have to be considered. The present work does not include these effects.

ACKNOWLEDGMENTS

We acknowledge Dr. A. Mehta of the University of Birmingham, U.K. and Dr. K. W. Brannon of IBM Almaden for providing the MARLOWE version which includes the spatially dependent target's electron density and BKK's energy-loss model pertinent to high energies. We also thank Donald Samuels for his help in digitizing the experimental data. One of us (C.S.M.) wishes to thank Dr. M. Robinson of Oak Ridge National Laboratory and Dr. L. R. Logan for useful discussions and comments on the manuscript.

[1]B. R. Appleton, C. Erginsoy, and W. M. Gibson, Phys. Rev. **161**, 330 (1967).
[2]Various articles in *Atomic Collision Phenomena in Solids,* edited by D. W. Palmer, M. W. Thompson, and P. D. Townsend (North-Holland, Amsterdam, 1970).
[3]G. Dearnaley, I. V. Mitchell, R. S. Nelson, B. W. Farmery, and M. W. Thompson, Philos. Mag. **18**, 985 (1968).
[4]F. H. Eisen, Can. J. Phys. **46**, 561 (1968).
[5]F. H. Eisen, G. J. Clark, J. Bottiger, and J. M. Poate, Radiat. Eff. **13**, 93 (1972).
[6]G. Della Mea, A. V. Drigo, S. Lo Russo, P. Mazzoldi, and G. G. Bentini, Radiat. Eff. **13**, 115 (1972).
[7]Yu. V. Bulgakov, V. S. Nikolaev, and V. I. Shugla, Phys. Status Solidi A **31**, 341 (1975).
[8]F. Bonsignori and A. Desalvo, Lett. Nuovo Cimento **1**, 589 (1969).
[9]F. Bonsignori and A. Desalvo, J. Phys. Chem. Solids **31**, 2191 (1970).
[10]A. Desalvo and R. Rosa, J. Phys. C **10**, 1595 (1977).
[11]F. F. Komarov and M. A. Kumakhov, Radiat. Eff. **22**, 1 (1974).
[12]A. F. Burenkov, F. F. Komarov, and M. A. Kumakhov, Phys. Status Solidi B **99**, 417 (1980).
[13]K. Dettmann and M. T. Robinson, Phys. Rev. B **10**, 1 (1974).
[14]K. Dettmann, Z. Phys. A **272**, 227 (1975).
[15]H. Esbensen and J. A. Golovchenko, Nucl. Phys. A **298** 382 (1978).
[16]M. T. Robinson and I. M. Torrens, Phys. Rev. B **9**, 5008 (1974).
[17]M. Hou and M. T. Robinson, Nucl. Instrum. Methods **132**, 641 (1976).
[18]M. T. Robinson, *Binary Collision Cascade Simulation Program Version 12 User's Guide* (Radiation Shielding Information Center, Oak Ridge National Laboratory, Oak Ridge, TN, 1984, Update Bulletin 5, 1988), pp. 1–115.
[19]M. Hane and M. Fukuma, IEDM Tech. Dig. **1988**, 648.
[20]M. Hautala, Nucl. Instrum. Methods B **15**, 75 (1986).
[21]B. J. Mulvaney, W. B. Richardson, and T. L. Crandle, IEEE Trans. Computer-Aided Des. **8**, 336 (1989).
[22]G. Hobler, H. Potzl, L. Palmetshofer, R. Schork, J. Lorenz, C. Tian, S. Gara, and G. Stingeder, in *The Seventh International Conference Proceeding on the Numerical Analysis of Semiconductor Device and Integrated Circuits,* edited by J. J. H. Miller (Front Range Press, Boulder, CO, 1991), Vol. VII, p. 85.
[23]M. T. Robinson, in *Sputtering by Particle Bombardment I,* edited by R. Behrisch (Springer, New York, 1981), Vol. 47, p. 83.
[24]D. E. Harrison, CRC Rev. Solid State Mater. Sci. **14**, S1 (1988), and references therein.
[25]W. Eckstein, in *Computer Simulation of Ion-Solid Interactions,* Springer Series in Materials Science Vol. 10 (Springer-Verlag, New York, 1991).
[26]C. S. Murthy and G. R. Srinivasan, IEEE Trans. Electron Devices **39**, 264 (1992).
[27]O. B. Firsov, Zh. Eksp. Teor. Fiz. **9**, 1517 (1959) [Sov. Phys. JETP **36**, 1076 (1959)].
[28]J. Lindhard and M. Scharff, Phys. Rev. **124**, 128 (1961).
[29]O. S. Oen and M. T. Robinson, Nucl. Instrum. Methods **132**, 647 (1976).
[30]N. Azziz, K. W. Brannon, and G. R. Srinivasan, in *Ion Beam Processes in Advanced Electronic Materials and Device Technology,* edited by B. R. Appleton, F. H. Eisen, and T. W. Sigmon, MRS Symposia Proceedings No. 45 (Materials Research Society, Pittsburgh, 1985), p. 71.
[31]K. M. Klein, C. Park, and A. F. Tasch, Appl. Phys. Lett. **57**, 2701 (1990).
[32]W. Brandt and M. Kitagawa, Phys. Rev. B **25**, 5631 (1982).
[33]W. Brandt, Nucl. Instrum. Methods **194**, 13 (1982).
[34]B. R. Appleton, C. D. Moak, T. S. Noggle, and B. J. H. Barrett, Phys. Rev. Lett. **28**, 1307 (1972).
[35]L. R. Logan, C. S. Murthy, and G. R. Srinivasan, Phys. Rev. A **46**, 5754 (1992).
[36]C. M. Bertoni, V. Bortolani, C. Calandra, and F. Nizzoli, J. Phys. C **6**, 3612 (1973).
[37]B. Dawson, Proc. R. Soc. London Ser. A **298**, 264 (1967).
[38]P. K. W. Vinsome and M. Jaros, J. Phys. C **4**, 1360 (1971).
[39]P. M. Raccah, R. N. Euwema, D. J. Stukel, and T. C. Collins, Phys. Rev. B **1**, 756 (1970).
[40]M. T. Robinson (private communication).
[41]M. T. Yin and M. L. Cohen, Phys. Rev. B **26**, 5668 (1982).
[42]C. Scheringer, Acta Crystallogr. Sec. A **36**, 205 (1980).
[43]J. Lindhard, K. Dan. Vidensk. Selsk. Mat. Fys. Medd. **28**, 8 (1954).

[44]J. Lindhard and M. Scharff, K. Dan. Vidensk. Selsk. Mat. Fys. Medd. **27**, 15 (1953).
[45]E. Bonderup and P. Hvelplund, Phys. Rev. A **4**, 562 (1971).
[46]P. Sigmund and De-Ji Fu, Phys. Rev. A **25**, 1450 (1982).
[47]W. K. Chu, Phys. Rev. A **13**, 2057 (1976).
[48]Y. Kido and T. Koshikawa, Phys. Rev. A **25**, 1759 (1991).
[49]T. Kaneko and Y. Yamura, Phys. Rev. A **33**, 1653 (1986).
[50]F. Besenbacher, J. U. Andersen, and E. Bonderup, Nucl. Instrum. Methods **168**, 1 (1980).
[51]P. Sigmund, in *Interaction of Charged Particles with Solids and Surfaces,* Vol. 270 of *NATO Advanced Study Institute Series B: Physics,* edited by A. Gras-Marti *et al.* (Plenum, New York, 1991).
[52]J. Oddershede and J. R. Sabin, At. Data Nucl. Data Tables **31**, 275 (1984).
[53]N. M. Kabachnik, V. N. Kondratev, and O. V. Chumanova, Phys. Status Solidi B **145**, 103 (1988).
[54]W. Both and J. S. Grant. Nucl. Phys. **63**, 481 (1965).
[55]C. F. Williamson, J. F. Boujot, and J. Picard, Rapport CEA R-3042 (1966).
[56]S. D. Bloom and G. D. Sauter, Phys. Rev. Lett. **26**, 607 (1971).
[57]H. D. Betz, Rev. Mod. Phys. **44**, 465 (1972).
[58]A. Arnau, M. Penalba, P. M. Echenqique, F. Flores, and R. H. Ritchie, Phys. Rev. Lett. **65**, 1024 (1990).
[59]E. Brandt, in *Atomic Collisions in Solids,* edited by S. Datz, B. R. Appleton, and C. D. Moak (Plenum, New York, 1975), Vol. 1, p. 261.
[60]C. S. Murthy, L. R. Logan, and G. R. Srinivasan, in *International Conference Proceeding on "Computer Simulations of Radiation Effects in Solids"–COSIRES 1992,* edited by J. P. Biersack and R. S. Averback (Gordon & Breach, New York, in press); Radiat. Eff. Defects Solids (to be published).
[61]Chr. Lehmann and G. Leibfried, Z. Phys. **172**, 465 (1963).